Laser and Particle Beams (2015), *33*, 347–353.

doi:10.1017/S026303461500018X

Self-shaping of a relativistic elliptically Gaussian laser beam in underdense plasmas

T. W. HUANG,[1] C. T. ZHOU,[2,3,4] AND X. T. HE[2,3]

[1]HEDPS, Center for Applied Physics and Technology and School of Physics, Peking University, Beijing, People's Republic of China
[2]HEDPS, Center for Applied Physics and Technology, Peking University, Beijing, People's Republic of China
[3]Institute of Applied Physics and Computational Mathematics, Beijing, People's Republic of China
[4]Science College, National University of Defense Technology, Changsha, People's Republic of China

(Received 30 August 2014; Accepted 9 February 2015)

Abstract

Self-shaping and propagation of intense laser beams of different radial profiles in plasmas is investigated. It is shown that when a relativistic elliptically Gaussian beam propagates through an underdense plasma, its radial profile will self-organize into a circularly symmetric self-similar smooth configuration. Such self-similar propagation can be attributed to a soliton-like structure of the laser pulse. The anisotropic electron distribution results in a circular electric field that redistributes the electrons and modulates the laser pulse to a circular radial shape.

Keywords: Relativistic elliptically Gaussian beam; Self-shaping; Soliton-like structure; Underdense plasmas

1. INTRODUCTION

Propagation of intense laser pulses at relativistic intensities through plasmas is of much interest in basic studies of laser–plasma interaction (LPI) and in its many potential applications (Yu *et al.*, 1978; 2000; Chen *et al.*, 1998; Fuchs *et al.*, 1998; 2005; Mourou *et al.*, 2006; Zhou & He, 2007; Hoffmann, 2008; Norreys, 2009; Norreys *et al.*, 2009; Qiao *et al.*, 2012), ranging from compact particle sources to new light sources, as well as for fast ignition in inertial confinement fusion. High-intensity laser beams propagating in underdense plasma can undergo self-focusing, self-channeling, as well as filamentation if its power exceeds the critical power P_{cr}~$17(\omega_L/\omega_p)^2$ GW, where ω_L and ω_p are the laser and plasma frequencies, respectively.

Self-focusing and self-channeling of relativistic laser pulse in plasmas have been extensively investigated both experimentally and numerically (Pukhov & Meyer-ter-Vehn, 1996; Borghesi *et al.*, 1997; Naseri *et al.*, 2010; 2012; Nilson *et al.*, 2010; Sylla *et al.*, 2013; Wang *et al.*, 2013). In the LPI, the laser ponderomotive force expels the electrons from the affected plasma region. The relativistic nonlinear Schrödinger equation (RNSE) that takes into account the relativistic ponderomotive effects has often been used for theoretical and numerical investigations of intense LPI in underdense plasmas (Sun *et al.*, 1987; Kurki-Suonio *et al.*, 1989; Borisov *et al.*, 1992; 1995; Chen & Sudan, 1993; Feit *et al.*, 1998; Hafizi *et al.*, 2000; Cattani *et al.*, 2001; Kim *et al.*, 2002; Qiao *et al.*, 2007*a*; 2007*b*). In the existing works, one usually considers lasers of circular cross-section with Gaussian radial intensity profile. However, in the experiments the laser cross-section is often non-circular, and their propagation characteristics can be quite different from that of the circular ones (Chen & Sudan, 1993). It is therefore of interest to investigate the effect of the radial laser profile on the propagation of intense lasers. In this paper, we consider the propagation of a relativistic laser beam of elliptic cross-section in underdense plasma. It is found that for certain parameter ranges the radial laser profile can become circularly symmetric and self-similar, regardless of its initial radial profile.

2. RNSE AND ITS BASIC PROPERTIES

If the duration τ of the laser pulse satisfies $\tau_i \gg \tau \gg \tau_e$, where τ_i and τ_e are the characteristic times of the ion and electron motion, the ion dynamics can be neglected. The electric field E of a circularly polarized laser propagating in a cold homogeneous plasma is given by RNSE (Sun *et al.*, 1987; Kurki-Suonio *et al.*, 1989; Borisov *et al.*, 1992; 1995; Chen & Sudan, 1993; Feit *et al.*, 1998; Hafizi

Address correspondence and reprint requests to: C. T. Zhou, Institute of Applied Physics and Computational Mathematics, Beijing 100094, People's Republic of China. E-mail: zcangtao@iapcm.ac.cn

et al., 2000; Cattani *et al.*, 2001; Kim *et al.*, 2002; Qiao *et al.*, 2007*a*; 2007*b*)

$$2ik_{\mathrm{L}}\frac{\partial}{\partial z}E+\nabla_{\perp}^{2}E+k_{\mathrm{p}}^{2}\left(1-\frac{n}{\gamma}\right)E=0, \tag{1}$$

in the frame moving at the laser group velocity, where z is the laser propagation direction and $\perp$ denotes the transverse direction, k_{L} is the laser wave vector, $k_{\mathrm{p}}=\omega_{\mathrm{p}}/c$, c is the vacuum light speed, $n=n_{\mathrm{e}}/n_0$ is the normalized electron density, n_0 is the background plasma density, $\gamma=\sqrt{1+|a|^2}$ is the relativistic parameter of an electron in a circularly polarized laser field, $a=eE/m_{\mathrm{e}}\omega_{\mathrm{L}}c$ is the normalized electric field, and m_{e} is the electron rest mass. The electron density is given by

$$n=1+k_{\mathrm{p}}^{-2}\nabla_{\perp}^{2}\gamma, \tag{2}$$

which is valid for $1+k_{\mathrm{p}}^{-2}\nabla_{\perp}^{2}\gamma>0$. For $1+k_{\mathrm{p}}^{-2}\nabla_{\perp}^{2}\gamma<0$, we usually replace n by 0 to ensure a positive density (Sun *et al.*, 1987). However in this case, the charge is not fully conserved in the presence of electron cavitation, which may make the quantitative results unreliable (Feit *et al.*, 1998; Hafizi *et al.*, 2000; Cattani *et al.*, 2001; Kim *et al.*, 2002). To ensure the charge conservation (CC), that is, $\int(n-1)dxdy=0$, one more condition should be satisfied

$$-k_{\mathrm{p}}^{-2}\nabla_{\perp}\gamma=R/2, \tag{3}$$

where R refers to the radius of the cavitation channel. However, Eqs. (1–3) cannot be used for simulation by itself. To make Eq. (1) consistent with the additional condition (3), a finite electron temperature T_{e} can be taken into account and then the electron density can be rewritten as (Feit *et al.*, 1998)

$$n=1+k_{\mathrm{p}}^{-2}\nabla_{\perp}^{2}(\gamma+\alpha\log_{\mathrm{e}}n), \tag{4}$$

where $\alpha=T_{\mathrm{e}}/m_{\mathrm{e}}c^2$ is the normalized electron temperature. In this case, a positive electron density is naturally ensured, as well as the CC condition. It is noted that the above equation is only valid for $\alpha\ll1$, which means that the thermal motion of electrons is non-relativistic.

For Eq. (1), there are infinite number of conserved quantities. The first invariant is the laser power $P=\int|a|^2dxdy$. If we assume that there is no electron cavitation initially, that is, $1+k_{\mathrm{p}}^{-2}\nabla_{\perp}^{2}\gamma>0$, the Hamiltonian can be expressed as $H=\int[|\nabla_{\perp}a|^2-k_{\mathrm{p}}^2(\gamma-1)^2-|\nabla_{\perp}\gamma|^2]\,dx\,dy$. Then the evolution of the laser spot $r^2\equiv\int(x^2+y^2)|a|^2dxdy/P$ is given by

$$\frac{d^2r^2}{dz^2}=\frac{2}{k_{\mathrm{L}}^2P}\left[H+k_{\mathrm{p}}^2\int\left(1-\frac{1}{\gamma}\right)(\gamma-1)^2dx\,dy+\int\left(\gamma-\frac{1}{\gamma}\right)(\nabla_{\perp}^{2}\gamma)dx\,dy\right], \tag{5}$$

where the last term on the right-hand side is due to the charge displacement driven by the ponderomotive force. When the right-hand side of Eq. (5) is less than zero, self-focusing can take place. For the non-relativistic case, that is, $a\ll1$, Eq. (5) reduces to

$$\frac{d^2r^2}{dz^2}=\frac{2H}{k_{\mathrm{L}}^2P}$$

with

$$H=\int\left[\left|\nabla_{\perp}a\right|^2-\frac{k_{\mathrm{p}}^2}{4}\left|a\right|^4\right]dx\,dy.$$

3. SELF-SHAPING OF A RELATIVISTIC ELLIPTICALLY GAUSSIAN LASER BEAM

For an initially elliptic Gaussian beam $a(x,y,0)=a_0\exp[-x^2/r_1^2-y^2/r_2^2]$, we can obtain the mean-square radius of the laser beam as

$$r^2=\frac{r_1r_2}{2}\left[1+\left(1-\frac{P_{\mathrm{in}}}{P_{\mathrm{cr},\theta}}\right)\frac{z^2}{z_{\mathrm{R}}^2}\right],$$

where $z_{\mathrm{R}}=k_{\mathrm{L}}r_1r_2/2$ is the Rayleigh length, $P_{\mathrm{cr},\theta}=P_{\mathrm{cr}}\cdot((\theta+1/\theta)/2)$ is the critical power for self-focusing, and $\theta=r_2/r_1(\geq1)$ is the ellipticity of the laser spot. Self-focusing occurs when $P_{\mathrm{in}}>P_{\mathrm{cr},\theta}$. The corresponding self-focusing distance ($z_{\mathrm{f}}\approx z_{\mathrm{R}}\sqrt{(P_{\mathrm{in}}/P_{\mathrm{cr},\theta})-1}$) is thus enhanced with increasing initial ellipticity. For the relativistic case, Eq. (5) does not lead to an analytical expression for r. However, one can easily solve Eq. (5) numerically.

We now solve the laser envelop Eq. (1) and the plasma density Eq. (4) numerically (He & Zhou, 1993; Zhou & He, 1994; Zhou *et al.*, 1994; Huang *et al.*, 2013). For the non-relativistic case, Eq. (1) reduces to the standard cubic nonlinear schrödinger equation (NSE), for which the Townes profile has been obtained numerically and experimentally (Gross & Manassah, 1992; Fibich & Ilan, 1999; Moll *et al.*, 2003; Dudley *et al.*, 2007). The input laser beam is modeled by an elliptic Gaussian profile

$$a(x,y,z=0)=a_0(1+\varepsilon)e^{-\left(\frac{x^2}{r_0^2\theta}+\frac{y^2}{r_0^2/\theta}\right)}, \tag{6}$$

where $a_0=8.85\times10^{-10}\sqrt{I_0\lambda^2(\mathrm{Wcm^{-2}\mu m^2})/2}$, I_0 is the peak laser intensity, r_0 is the initial beam waist, θ is the initial beam ellipticity, and ε denotes the random noise added to the profile, given by random numbers from the computer. In our simulation, the central laser wavelength is assumed to be 1 μm and initial beam waist is 6 μm. In addition, we consider the laser power ($P_{\mathrm{in}}=I_0\pi r_0^2/2$) ranges from $1P_{\mathrm{cr}}$ to $20P_{\mathrm{cr}}$ and the initial plasma density is $0.02n_{\mathrm{c}}$, where n_{c} is the critical plasma density. The normalized electron temperature is set as $\alpha=0.02$. The maximum noise level is $\max(\varepsilon)\leqslant0.1$.

https://doi.org/10.1017/S026303461500018X Published online by Cambridge University Press

A solution of Eqs. (1) and (4) corresponding to $P_{in}/P_{cr} = 1.9$ and $r_0 k_p = 5.3$ is shown in Figure 1. Figure 1a–1c present the propagation behavior of an initial randomly distorted circular beam. It is shown that the beam profile gradually becomes smooth during the self-focusing process and the peak laser intensity reaches its largest value at $z \approx 120$ μm. We also consider the elliptical cases with $\theta = 1.5$ and 3, respectively, as shown in Figure 1d–1i. It can be seen from Figure 1f and 1i that even if the initial beam is highly elliptical and randomly distorted, a smooth and circular beam can still be produced by the self-focusing process in plasmas. Such a behavior would be of great interest for laser shaping applications.

The shaping process can be understood from the distribution of the refractive index $\eta = (1-(n_e/n_c\gamma))^{1/2}$ and its gradient in transverse place represents the direction of laser energy flow. For an initially circular beam ($\theta = 1$), gradient of the refractive index can be expressed as $|\nabla_\perp \eta| = (d\eta/dr)$, suggesting that the energy flow is isotropic, as shown in Figure 2a, and the radial shape shall keep on circular during the propagation process. However, for the elliptical case with $\theta > 1$,

$$|\nabla_\perp \eta| = \sqrt{\left(\frac{\partial \eta}{\partial r}\right)^2 + \left(\frac{1}{r}\frac{\partial \eta}{\partial \varphi}\right)^2},$$

where φ is the angular variable and the anisotropic part $(\partial\eta/\partial\varphi)$ contributes to the change of the radial shape from an elliptical case to a circular case. Specially, it is shown from Figure 2b that due to stronger ponderomotive force, electrons are piled up in the minor axis at first and the steep electron walls can provide strong focusing effect to confine the laser energy in the minor axis. A balance between the diffraction and the focusing effect can be first achieved in the minor axis and the peripheral energy would converge into the major axis, as shown in Figure 2b. Then at the self-focusing distance, the intensity profile gradually evolves into a circular shape, in which the nonlinear focusing effect and diffraction precisely balance each other. On the other hand, we can understand the self-shaping process in microscopic view by considering the motion of electrons in transverse place. Once the initial laser beam profile is deviated from the circular case, the resulting anisotropic distributed electrons will induce an additional circumferential electric field, and it is noted that such an electric field tends to make the electrons be isotropic distributed, which in turn would self-consistently modulate the radial profile of the laser beam to a circular shape. Our simulations further demonstrate that the self-shaping process is periodic and the circular profile is produced at each self-focusing point. In addition, it is seen from Figure 1 that the self-focusing distance increases with the ellipticity of the input laser beam, that is, the farther the initial beam deviates from the circular case, the longer the beam has to propagate in order to have the circular profile. This result is in good agreement with our theory given earlier.

To further describe the physical processes of our three cases as shown in Figure 1, we in Figure 3 give a detailed comparison of different radial profiles of the intensity patterns. It is seen from Figure 3a that the central portions of the laser beams are of a circular shape at the self-focusing distance and they almost overlap together for different elliptical cases, suggesting that the self-focusing process in plasmas is self-similar, that is, the output beam profile after the self-shaping process is not relevant to the initial laser beam profile. However, it is noted that the periphery of the beam in the transverse directions cannot completely overlap (see Fig. 3b) for the $\theta > 1$ case due to the anisotropic diffraction (Gross & Manassah, 1992; Fibich & Ilan, 1999; Moll *et al.*, 2003; Dudley *et al.*, 2007).

The self-similar profile as shown in Figure 3a and 3b is associated with their corresponding stationary solutions. For Eq. (1), an axisymmetric stationary solution can be expressed as $a(r, z) = a_s(r)exp[i(k_p^2/2k_L)(1 - S)z]$, where $a(r,z)$ is the normalized electric field as defined above and S is a real constant parameter. Substituting it into Eq. (1) we can obtain the eigen equation for a_s

$$\left(\frac{d^2}{dr^2} + \frac{1}{r}\frac{d}{dr}\right)a_s + k_p^2\left(S - \frac{n}{\sqrt{1+|a_s|^2}}\right)a_s = 0. \qquad (7)$$

In addition, a_s is subject to the boundary conditions

$$\frac{da_s(r)}{dr}|_{r=0} = 0$$

and $\lim_{r\to\infty} a_s(r) = 0$. The condition $0 < S < 1$ should also be satisfied to obtain a non-zero solution. Considering the cavitation case ($P_{in}/P_{cr} > 1.1$), we can then separate Eq. (7) into two parts. In the region without electron cavitation, Eq. (7) can be expressed as

$$\left(\frac{d^2}{dr^2} + \frac{1}{r}\frac{d}{dr}\right)a_s + k_p^2\left(S - \frac{1}{\sqrt{1+|a_s|^2}}\right)a_s = 0.$$

and its asymptotic solution at infinity can be written as $a_s(r \to \infty) = \beta\sqrt{1/(\kappa k_p r)}e^{-\kappa k_p r}$, where β is a real constant parameter and $\kappa = \sqrt{1-S}$. In the region with electron cavitation ($r < R$), Eq. (7) is replaced by

$$\left(\frac{d^2}{dr^2} + \frac{1}{r}\frac{d}{dr}\right)a_s + k_p^2 S a_s = 0,$$

and its solution is simply the zeroth-order Bessel function $a_s(r) = a_s(0)J_0(S^{1/2}k_p r)$. To ensure the CC, the condition (3) should also be satisfied at the boundary R. By inserting $a_s(R)$ into Eq. (3), we have the amplitude $a_s(0)$ as a function

https://doi.org/10.1017/S026303461500018X Published online by Cambridge University Press

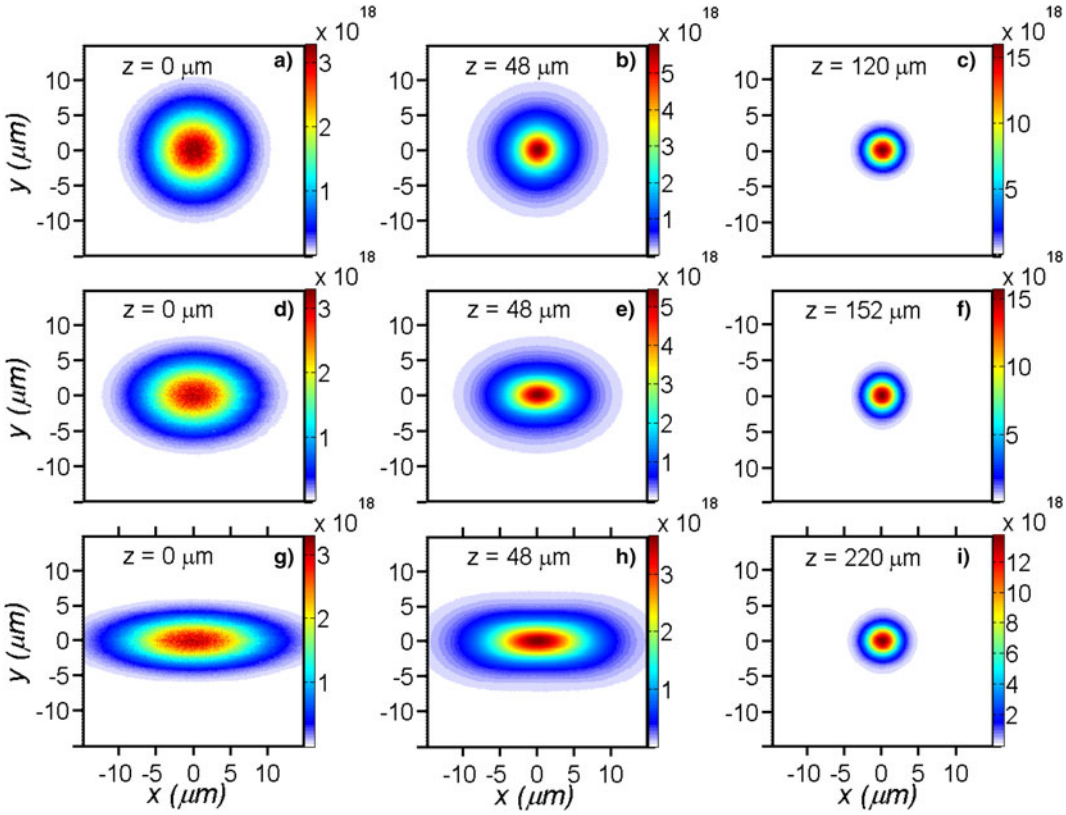

Fig. 1. Evolution of different elliptical Gaussian laser beams with an initial 10% random noise in transverse space. (a–c) are the intensity patterns at different propagation distances for $\theta = 1$, (d–f) are for $\theta = 1.5$, and (g–i) are for $\theta = 3$. The unit of laser intensity is W/cm^2. The displayed space scale is 30×30 μm and the simulation box is 50×50 μm. The normalized electron temperature is set as $\alpha = 0.02$ in the simulations.

of S and R (Cattani *et al.*, 2001)

$$a_s(0)^2 = \frac{k_p^2 R^2}{8SJ_1^2(\sqrt{S}k_p R)}\left(1+\sqrt{1+\frac{16SJ_1^2(\sqrt{S}k_p R)}{R^2 J_0^2(\sqrt{S}k_p R)}}\right), \quad (8)$$

where J_1 refers to the first-order Bessel function. Then the lowest eigenmode solution in Eq. (7) can be obtained numerically using the shooting method. It can be seen from Figure 3c and 3d that if the total CC is satisfied, the lowest eigenmode solution possesses a lower amplitude and a wider channel radius at

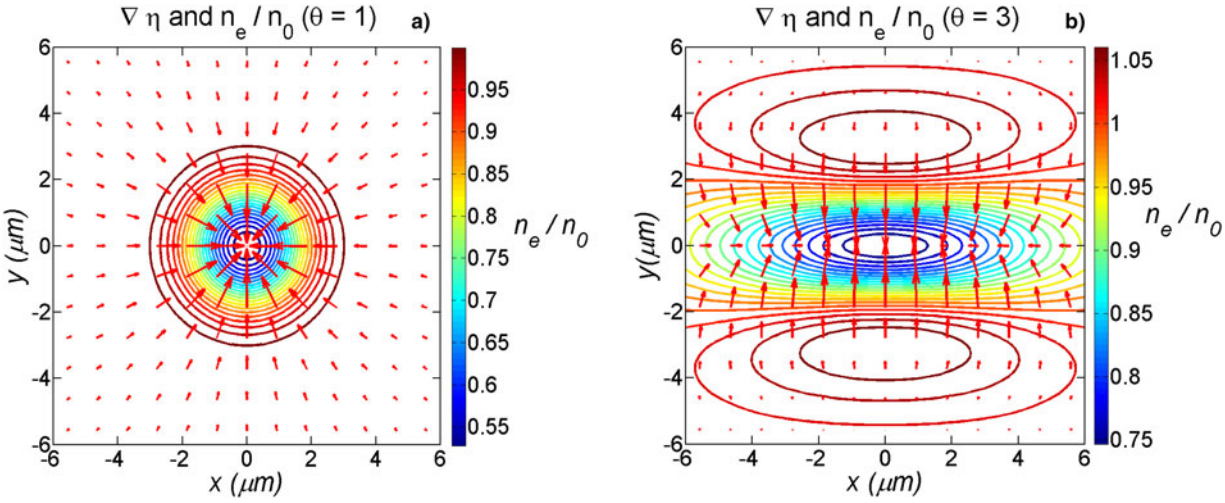

Fig. 2. The gradient of the refractive index and contour of the plasma density for the case of $\theta = 1$ (a) and $\theta = 3$ (b), where their intensity contours correspond to Figure 1b and 1h, respectively.

https://doi.org/10.1017/S026303461500018X Published online by Cambridge University Press

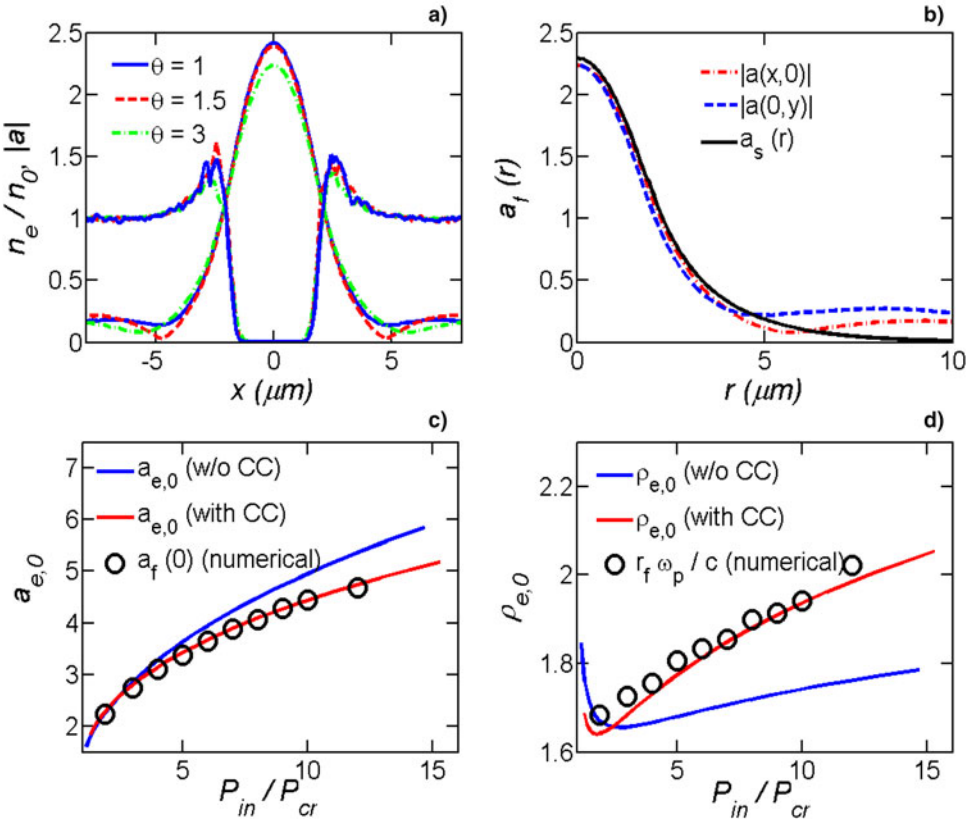

Fig. 3. (a) is the profile of the normalized electric field and plasma density along *X*-axis for different elliptical cases, which are corresponding to the intensity patterns shown in Figure 1c, 1f, and 1i. (b) gives a comparison of intensity profiles shown in Figure 1i along two different directions with the soliton solution of Eq. (7) for θ = 3. Panels (c) and (d) are, respectively, the scalings of the amplitude and the normalized radius of the self-similar profile with different input powers, where the circles in the figures are numerical results from Eqs. (1) and (4) for θ = 3 case and the solid line is theoretical results computed from Eq. (7), where the blue one corresponds to case without CC and the red one corresponds to case with CC [Eq. (8)]. $a_{e,0}$ and $\rho_{e,0}$ in the figures denote the amplitude and normalized radius of the lowest eigenmode respectively.

a fixed laser power. On the other hand, it was showed that the lowest eigenmode can act as a soliton and maintain its shape when the soliton-like beam propagates through the plasmas (Sun *et al.*, 1987; Kurki-Suonio *et al.*, 1989). For the system with soliton solutions, it is well known that if the initial state is slightly different from the soliton solution, the beam profile would oscillate around the stable state. In our case, it is shown from Figure 3b that the central portion of the self-shaped profile is in a good match with the soliton solution of Eq. (7). Furthermore, in Figure 3c and 3d, we give a comparison of the amplitude [$a_f(0)$] and the radius of the self-similar beam [$r_f = \sqrt{2P_{in}/a_f(0)^2}$] with the corresponding theoretical values of the lowest eigenmode of Eq. (7) at different input powers. It is shown that our numerical results agree well with our theoretical results. In addition, it is noted that the numerical results computed from the thermal correction model [Eqs. (1) and (4)] match well with the lowest eigenmode solution considering the CC instead of the non-conservation case. Such a conclusion is suitable for $\alpha < 0.1$. Our scalings of both the amplitude of the self-similar profile $a_f(0)$ and the normalized radius $r_f\omega_p/c$ with the normalized power (P_{in}/P_{cr}) clearly demonstrate that the self-similar behavior shown in Figure 1 is actually determined by the lowest eigenmode in Eq. (7). In other words, during the self-focusing process the intensity profile of the laser beam would asymptotically evolve into its corresponding eigenmode. The soliton-like eigenmode then acts as a robust attractor to make the self-shaping process occur spontaneously.

Now some illustrations on the university of the self-similar behavior should be made. It had been found that for relativistic laser pulses propagating in underdense plasmas, its propagation behavior mainly depends on two dimensionless parameters, that is, the normalized radius ($r_0\omega_p/c$) and the normalized power (P_{in}/P_{cr}) of the input laser beam (Borisov *et al.*, 1992; 1995). The stability map for an initial circularly distributed relativistic laser beam propagating in underdense plasmas is shown in Figure 4. It is demonstrated that the laser beam would suffer from the filamentation instability and break up into serval filaments when both the radius and power of the beam are large enough, as shown in the inset. While the yellow region in Figure 4 corresponds to the stable region and it is noted that the self-similar behavior

https://doi.org/10.1017/S026303461500018X Published online by Cambridge University Press

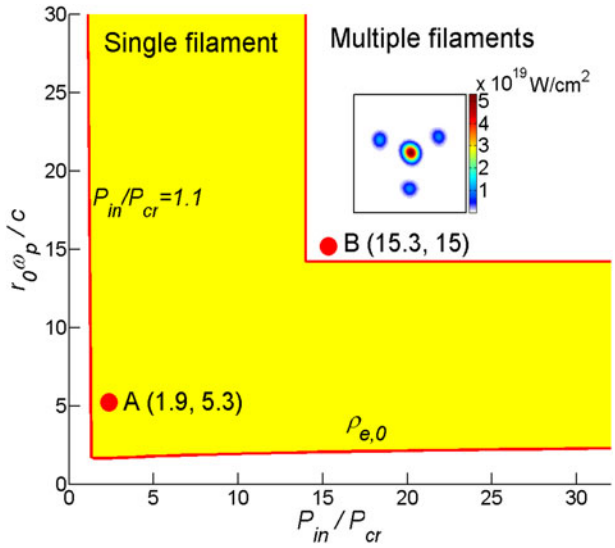

Fig. 4. Stability map for the propagation of an initial circularly distributed relativistic Gaussian beam in homogeneous underdense plasmas, where the lower boundary is the radius of the lowest eigenmode in Eq. (7) considering the CC [Eq. (8)] and the left boundary refers to the condition of electron cavitation ($P_{in} > 1.1P_{cr}$). The horizontal axis is the normalized laser power and the longitudinal axis is the normalized radius of the input laser beam. The yellow region in the map corresponds to the stable region with single filament and the above blank region is the unstable region with multiple filaments. An example of the multiple filament patterns corresponding to the B point is shown in the inset.

only occurs in this region, that is, an initial arbitrary shaped laser beam in the yellow region would collapse towards its corresponding soliton solution for a fixed normalized laser power (P_{in}/P_{cr}).

Understanding the self-shaping mechanism of self-focusing laser beams propagating in plasmas is not only of fundamental interest but is also important for many applications in LPI (Yu *et al.*, 1978; 2000; Chen *et al.*, 1998; Fuchs *et al.*, 1998; 2005; Mourou *et al.*, 2006; Zhou & He, 2007; Hoffmann, 2008; Norreys, 2009; Norreys *et al.*, 2009; Qiao *et al.*, 2012). Especially, many potential applications depend strongly on the beam quality, including the intensity and the transverse profile of the laser spot. For example, in relativistic laser-driven particle sources, the maximum proton energy driven by the target normal sheath acceleration mechanism (Mora, 2003) as well as the temperature of hot electrons accelerated from a solid target (Wilks *et al.*, 1992) is scaled as $\propto I^{1/2}$. Furthermore, both the energy and angle spectra depend on the intensity and the transverse distribution of the laser spot (Mourou *et al.*, 2006; Zhou & He, 2007). Figure 1 shows that an initial elliptical laser beam can self-organize into a circularly symmetric self-similar smooth beam. The corresponding peak laser intensity is approximately enhanced by a factor of 4. In other words, the cut-off energy of the laser-accelerated protons and the temperature of hot electrons may be increased by a factor of approximately 2 if a proper underdense plasma is put in front of the solid target. The key is to ensure that the reshaped pulse has a higher intensity and a better radial profile before the laser beam interacts with the solid target.

4. CONCLUSIONS

In summary, self-focusing of a relativistic elliptical Gaussian laser beam in underdense plasmas with different values of the ellipticity is investigated. It is found that a self-similar, smooth, and circularly symmetric pattern of the self-shaped beam can be formed regardless of its initial radial profile. The transverse ponderomotive force of the elliptical laser beam in both short- and long axes can lead to the electrons being redistributed around the beam and self-shaping the laser field into a circular structure by nonlinear self-organization processes. Our theoretical results show that the central portion of the intensity profile of the self-shaped beam in self-focusing processes can approximately be described according to a soliton-like profile. Such a self-shaped laser pulse beam can be of many potential applications in relativistic high-energy density plasmas.

ACKNOWLEDGEMENTS

This work is supported by the National Natural Science Foundation of China (grant no. 91230205 and 11175026), the National Basic Research 973 Project, No. 2013CB834100, and the National High-Tech 863 Project. T. W. H. would like to thank H. Zhang, S. Z. Wu, F. L. Zheng, T. P. Yu, H. B. Zhuo, C. Z. Xiao, Q. Jia, D. Wu, H. Y. Wang, and B. Liu for their useful helps and discussions.

REFERENCES

Borghesi, M., MacKinnon, A.J., Barringer, L., Gaillard, R., Gizzi, L.A., Meyer, C., Willi, O., Pukhov, A. & Meyer-ter-Vehn, J. (1997). Relativistic channeling of a picosecond laser pulse in a near-critical preformed plasma. *Phys. Rev. Lett.* **78**, 879–882.

Borisov, A.B., Borovskiy, A.V., Mcpherson, A., Boyer, K. & Rhodes, C.K. (1995). Stability analysis of relativistic and charge-displacement self-channelling of intense laser pulses in underdense plasmas. *Plasma Phys. Control. Fusion* **37**, 569–597.

Borisov, A.B., Borovskiy, A.V., Shiryaev, O.B., Korobkin, V.V., Prokhorov, A.M., Solem, J.C., Luk, T.S., Boyer, K. & Rhodes, C.K. (1992). Relativistic and charge-displacement self-channeling of intense ultrashort laser pulses in plasmas. *Phys. Rev. A* **45**, 5830–5845.

Cattani, F., Kim, A., Anderson, D. & Lisak, M. (2001). Multifilament structures in relativistic self-focusing. *Phys. Rev. E* **64**, 016412(1–8).

Chen, S.Y., Sarkisov, G.S., Maksimchuk, A., Wagner, R. & Umstadter, D. (1998). Evolution of a plasma waveguide created during relativistic-ponderomotive self-channeling of an intense laser pulse. *Phys. Rev. Lett.* **80**, 2610–2613.

Chen, X.L. & Sudan, R.N. (1993). Necessary and suffcient conditions for self-focusing of short ultraintense laser pulse in underdense plasma. *Phys. Rev. Lett.* **70**, 2082–2085.

https://doi.org/10.1017/S026303461500018X Published online by Cambridge University Press

Dudley, J.M., Finot, C., Richardson, D.J. & Millot, G. (2007). Self-similarity in ultrafast nonlinear optics. *Nat. Phys*. **3**, 597–603.

Feit, M.D., Komashko, A.M., Musher, S.L., Rubenchik, A.M. & Turitsyn, S.K. (1998). Electron cavitation and relativistic self-focusing in underdense plasma. *Phys. Rev. E* **57**, 7122–7125.

Fibich, G. & Ilan, B. (1999). Self-focusing of elliptic beams: An example of the failure of the aberrationless approximation. *J. Opt. Soc. Am. B* **17**, 1749–1758.

Fuchs, J., Malka, G., Adam, J.C., Amiranoff, F., Baton, S.D., Blanchot, N., Héron, A., Laval, G., Miquel, J.L., Mora, P., Pépin, H. & Rousseaux, C. (1998). Dynamics of subpicosecond relativistic laser pulse self-channeling in an underdense preformed plasma. *Phys. Rev. Lett*. **80**, 1658–1661.

Fuchs, J., Sentoku, Y., Karsch, S., Cobble, J., Audebert, P., Kemp, A., Nikroo, A., Antici, P., Brambrink, E., Blazevic, A., Campbell, E.M., Fernández, J.C., Gauthier, J.C., Geissel, M., Hegelich, M., Pépin, H., Popescu, H., Renard-LeGalloudec, N., Roth, M., Schreiber, J., Stephens, R. & Cowan, T.E. (2005). Comparison of laser ion acceleration from the front and rear surfaces of thin foils. *Phys. Rev. Lett*. **94**, 045004(1–4).

Gross, B. & Manassah, J.T. (1992). Numerical solution for the propagation of an elliptic Gaussian beam in a Kerr medium. *Phys. Lett. A* **169**, 371–378.

Hafizi, B., Ting, A., Sprangle, P. & Hubbard, R.F. (2000). Relativistic focusing and ponderomotive channeling of intense laser beams. *Phys. Rev. E* **62**, 4120–4125.

He, X.T. & Zhou, C.T. (1993). Spatiotemporal complexity of the cubic-quintic nonlinear Schrödinger equation. *J. Phys. A* **26**, 4123–4133.

Hoffmann, D.H.H. (2008). Laser interaction with matter and heavy ion fusion. *Laser Part. Beams* **26**, 509–510.

Huang, T.W., Zhou, C.T. & He, X.T. (2013). Pattern dynamics and filamentation of femtosecond terawatt laser pulses in air including the higher-order Kerr effects. *Phys. Rev. E* **87**, 053103(1–19).

Kim, A., Tushentsov, M., Cattani, F., Anderson, D. & Lisak, M. (2002). Axisymmetric relativistic self-channeling of laser light in plasmas. *Phys. Rev. E* **65**, 036416(1–10).

Kurki-Suonio, T., Morrison, P.J. & Tajima, T. (1989). Self-focusing of an optical beam in a plasma. *Phys. Rev. A* **40**, 3230–3239.

Moll, K.D., Gaeta, A.L. & Fibich, G. (2003). Self-similar optical wave collapse: Observation of the townes profile. *Phys. Rev. Lett*. **90**, 203902(1–4).

Mora, P. (2003). Plasma expansion into a vacuum. *Phys. Rev. Lett*. **90**, 185002(1–4).

Mourou, G.A., Tajima, T. & Bulanov, S.V. (2006). Optics in the relativistic regime. *Rev. Mod. Phys*. **78**, 309–371.

Naseri, N., Bychenkov, V.Y. & Rozmus, W. (2010). Axial magnetic field generation by intense circularly polarized laser pulses in underdense plasmas. *Phys. Plasmas* **17**, 083109(1–10).

Naseri, N., Pesme, D., Rozmus, W. & Popov, K. (2012). Channeling of relativistic laser pulses, surface waves, and electron acceleration. *Phys. Rev. Lett*. **108**, 105001(1–4).

Nilson, P.M., Mangles, S.P.D., Willingale, L., Kaluza, M.C., Thomas, A.G.R., Tatarakis, M., Clarke, R.J., Lancaster, K.L., Karsch, S., Schreiber, J., Najmudin, Z., Dangor, A.E. & Krushelnick, K. (2010). Plasma cavitation in ultraintense laser interactions with underdense helium plasmas. *New J. Phys*. **12**, 045014(1–10).

Norreys, P.A. (2009). Laser-driven particle acceleration. *Nat. Photonics* **3**, 423–425.

Norreys, P.A., Scott, R.H.H., Lancaster, K.L., Green, J.S., Robinson, A.P.L., Sherlock, M., Evans, R.G., Haines, M.G., Kar, S., Zepf, M., Key, M.H., King, J., Ma, T., Yabuuchi, T., Wei, M.S., Beg, F.N., Nilson, P., Theobald, W., Stephens, R.B., Valente, J., Davies, J.R., Takeda, K., Azechi, H., Nakatsutsumi, M., Tanimoto, T., Kodama, R. & Tanaka, K.A. (2009). Recent fast electron energy transport experiments relevant to fast ignition inertial fusion. *Nucl. Fusion* **49**, 104023(1–8).

Pukhov, A. & Meyer-ter-Vehn, J. (1996). Relativistic magnetic self-channeling of light in near-critical plasma: Three-dimensional particle-in-cell simulation. *Phys. Rev. Lett*. **76**, 3975–3978.

Qiao, B., Kar, S., Geissler, M., Gibbon, P., Zepf, M. & Borghesi, M. (2012). Dominance of radiation pressure in ion acceleration with linearly polarized pulses at intensities of 10^{21} W/cm^2. *Phys. Rev. Lett*. **108**, 115002(1–5).

Qiao, B., Lai, C.H., Zhou, C.T., He, X.T. & Wang, X.G. (2007*a*). Complex dynamics of femtosecond terawatt laser pulses in air. *Appl. Phys. Lett*. **91**, 221114(1–3).

Qiao, B., Lai, C.H., Zhou, C.T., He, X.T., Wang, X.G. & Yu, M.Y. (2007*b*). Nonlinear properties of relativistically intense laser in plasmas. *Phys. Plasmas* **14**, 112301(1–7).

Sun, G.Z., Ott, E., Lee, Y.C. & Guzdar, P. (1987). Self-focusing of short intense pulses in plasmas. *Phys. Fluids* **30**, 526–532.

Sylla, F., Flacco, A., Kahaly, S., Veltcheva, M., Lifschitz, A., Malka, V., dHumières, E., Andriyash, I. & Tikhonchuk, V. (2013). Short intense laser pulse collapse in near-critical plasma. *Phys. Rev. Lett*. **110**, 085001(1–5).

Wang, H.Y., Lin, C., Sheng, Z.M., Liu, B., Zhao, S., Guo, Z.Y., Lu, Y.R., He, X.T., Chen, J.E. & Yan, X.Q. (2013). Laser shaping of a relativistic intense, short Gaussian pulse by a plasma lens. *Phys. Rev. Lett*. **107**, 265002(1–5).

Wilks, S.C., Kruer, W.L., Tabak, M. & Langdon, A.B. (1992). Absorption of ultra-intense laser pulses. *Phys. Rev. Lett*. **69**, 1383–1386.

Yu, M.Y., Shukla, P.K. & Spatschek, K.H. (1978). Localization of high-power laser pulses in plasmas. *Phys. Rev. A* **18**, 1591–1596.

Yu, W., Bychenkov, V., Sentoku, Y., Yu, M.Y., Sheng, Z.M. & Mima, K. (2000). Electron acceleration by a short relativistic laser pulse at the front of solid targets. *Phys. Rev. Lett*. **85**, 570–573.

Zhou, C.T. & He, X.T. (1994). Spatial chaos and patterns in laser-produced plasmas. *Phys. Rev. E* **49**, 4417–4424.

Zhou, C.T. & He, X.T. (2007). Influence of a large oblique incident angle on energetic protons accelerated from solid-density plasmas by ultraintense laser pulses. *Appl. Phys. Lett*. **90**, 031503(1–3).

Zhou, C.T., He, X.T. & Cai, T.X. (1994). Pattern structures on generalized nonlinear Schrödinger equations with various nonlinear terms. *Phys. Rev. E* **50**, 4136–4155.